

Dalton Transactions

Accepted Manuscript



This is an *Accepted Manuscript*, which has been through the Royal Society of Chemistry peer review process and has been accepted for publication.

Accepted Manuscripts are published online shortly after acceptance, before technical editing, formatting and proof reading. Using this free service, authors can make their results available to the community, in citable form, before we publish the edited article. We will replace this *Accepted Manuscript* with the edited and formatted *Advance Article* as soon as it is available.

You can find more information about *Accepted Manuscripts* in the [Information for Authors](#).

Please note that technical editing may introduce minor changes to the text and/or graphics, which may alter content. The journal's standard [Terms & Conditions](#) and the [Ethical guidelines](#) still apply. In no event shall the Royal Society of Chemistry be held responsible for any errors or omissions in this *Accepted Manuscript* or any consequences arising from the use of any information it contains.



Dual emission tunable in the near-infrared (NIR) and visible (VIS) spectral range by Mix-LnMOF

rReceived 00th January 20xx,
Accepted 00th January 20xx

DOI: 10.1039/x0xx00000x

www.rsc.org/

Roberta Anjos de Jesus^a, Leonis Lourenço da Luz^b, Danilo Oliveira Santos^a, José Arnaldo Santana Costa^a, Sandro Navickiene^a, Claudia Cristina Gatto^c, Severino Alves Júnior^{b*} and Maria Eliane de Mesquita^a.

In this work, we describe the synthetic approach, crystallographic structure, luminescent behavior and elucidate the channels of the energy conversion in heteronuclear coordination polymers with emission in the visible (Eu³⁺ and organic ligand) and near-infrared (Nd³⁺) range. The [(Nd_{0.9}Eu_{0.1})₂(dipc)₃(H₂O)₃]_n·nH₂O, [(Nd_{0.7}Eu_{0.3})₂(dipc)₃(H₂O)₃]_n·nH₂O, [(Nd_{0.5}Eu_{0.5})₂(dipc)₃(H₂O)₃]_n·nH₂O, [(Nd_{0.3}Eu_{0.7})₂(dipc)₃(H₂O)₃]_n·nH₂O, [(Nd_{0.1}Eu_{0.9})₂(dipc)₃(H₂O)₃]_n·nH₂O, [Eu₂(dipc)₃(H₂O)₃]_n·nH₂O and [Nd₂(dipc)₃(H₂O)₃]_n·nH₂O materials are obtained by hydrothermal conditions from pyridine-2,6-dicarboxylic acid (H₂dipc) and respective Ln₂O₃ oxide (Ln = Eu and Nd). The fine structure of emission spectrum and spectral profile are used to investigate the ion responsible for emission characteristic of (6) material, based on coordination polyhedron. The heteronuclear systems show emission in dual spectral range (NIR-VIS) tuned for blue or red. The tuning of emission on the red (Eu³⁺) or blue (organic ligand) range may be performed by stoichiometric ratio control between the lanthanide ions and by excitation wavelength. Nd³⁺ ions display self-absorption of emission to dipc ligand resulting in interference on the emission band profile ranging from 400 to 600 nm. The energetic process of energy transfer is operated by a cascade of energy transfer, from dipc ligand mainly to Eu³⁺ ions and finishing on the Nd³⁺ ion. The efficient sensitization to Nd³⁺ by Eu³⁺ ions is due to the presence of many resonant energy levels and short distance between these ions.

Introduction

In the last two decades, the development of multifunctional supramolecular devices based on coordination polymers, has been driven by intrinsic properties of their individual precursor materials and unique properties due to their synergism in the end structure, such as luminescence in large spectral range, magnetic behaviour, porosity, selective adsorption, catalysis and others.¹⁻⁶ The employment of mixing and co-doping of different metal types is a commonly used approach to obtain coordination polymers with large spectral range emission for applications in luminescent sensing and light-emitting.^{2, 7-10} Lanthanide trivalent ions shows narrow line-like emission bands from *f-f* states. This results in a large number of the absorption and emission bands arising from the transitions

between the energy levels, covering spectral range from near ultraviolet (NUV) to near-infrared (NIR).^{11,12} These intrinsic luminescent properties of lanthanide ions, together with the unique advantages of coordination polymers, offer excellent prospects for designing novel luminescent materials with high added values for specific applications in telecommunications, medical diagnoses, and so on.¹³⁻¹⁷ Mixed-lanthanide systems were traditionally used in matrix composition to actuate as sensitizer in up-conversion systems and in white light emission devices.^{10,18-21} However, other reports present the development of systems with dual and bimodal emission (UV/VIS/NIR), based on heterolanthanide cationic species, [Ln(H₂O)₈]³⁺, encapsulated in supramolecular systems.²²⁻²⁴ The development of dual emissive materials based on heteronuclear *f-f* arrays with different lanthanide ions made it possible to develop advanced technological applications such as ratiometric thermometers, markers, clinical diagnostics and other optical sensors.^{10, 25-31} One limitation on design of mixed/co-doping-lanthanide-organic material, containing two or more independent luminophore, is due to randomized distribution to lanthanide ions. This behaviour results in a distribution of distinct populations with crystal domain composed by only europium ions, by only neodymium ions and by co-doped domain. In addition, it is verified the large incidence to energy transfer and energy migration between the multi-luminophore resulting in emission quenching.^{8, 32-34}

^a Department of Chemistry, UFS, 49100-000, São Cristóvão-SE, Brazil

^b Department of Fundamental Chemistry, UFPE, 50.740-560, Recife – PE, Brazil. Tel. +55 81 2126-7475; e-mail: salvesjr@ufpe.br

^c University of Brasilia (IQ-UnB), campus Universitário Darcy Ribeiro, CEP 70904970, P.O. Box 4478, Brasília-DF, Brazil.

CCDC 1404007 and 1404008 contain the supplementary crystallographic data for this paper. These data can be obtained free of charge from The Cambridge Crystallographic Data Centre via www.ccdc.com.ac.uk/data_request/cif.

† Electronic supplementary information (ESI) available: Powder XRD patterns, thermogravimetric and elemental analyse, porosity characteristics, SEM images, additional structural, photo-luminescence measurements, as well as a table with important crystallographic data. For ESI see DOI: 10.1039/x0xx00000x

However, by controlling the stoichiometry ratio of the reactants we can obtain mixed-MOFs with any desired lanthanide composition and in a predictable and reproducible fashion, thus opening a convenient pathway for tuning luminescence properties of MOFs. This study describes the synthesis, characterization and spectroscopic evaluation of five new coordination polymers containing mixed-lanthanide ions (Mixed-LnMOF) and the materials containing only one ion type. We consider the formula of these materials based on stoichiometric ratio of reaction as $[(\text{Nd}_{0.9}\text{Eu}_{0.1})_2(\text{dipic})_3(\text{H}_2\text{O})_3]_n \cdot n\text{H}_2\text{O}$, $[(\text{Nd}_{0.7}\text{Eu}_{0.3})_2(\text{dipic})_3(\text{H}_2\text{O})_3]_n \cdot n\text{H}_2\text{O}$, $[(\text{Nd}_{0.5}\text{Eu}_{0.5})_2(\text{dipic})_3(\text{H}_2\text{O})_3]_n \cdot n\text{H}_2\text{O}$, $[(\text{Nd}_{0.3}\text{Eu}_{0.7})_2(\text{dipic})_3(\text{H}_2\text{O})_3]_n \cdot n\text{H}_2\text{O}$, $[(\text{Nd}_{0.1}\text{Eu}_{0.9})_2(\text{dipic})_3(\text{H}_2\text{O})_3]_n \cdot n\text{H}_2\text{O}$, $[\text{Eu}_2(\text{dipic})_3(\text{H}_2\text{O})_3]_n \cdot n\text{H}_2\text{O}$ and $[\text{Nd}_2(\text{dipic})_3(\text{H}_2\text{O})_3]_n \cdot n\text{H}_2\text{O}$, herein designed as **(1)**, **(2)**, **(3)**, **(4)**, **(5)**, **(6)** and **(7)**, respectively, and dipic is pyridine-2,6-dicarboxylate ion. Dipicolinic acid was chosen, due their ability and diversity of coordinations mode, resulting a large number of reported structures, and also systems containing heteronuclear f-f arrays with different lanthanide ions.³⁴⁻³⁸

Experimental Section

Chemicals and Reactants. Neodymium (III) oxide (Nd_2O_3) (99.99%), europium (III) oxide (Eu_2O_3) (99.99%) and pyridine-2,6-dicarboxylic acid (H_2dipic) (99%) from Aldrich (USA), were used as received and without further purification.

Synthesis. The coordination compounds $[(\text{Nd}_x\text{Eu}_{1-x})_2(\text{dipic})_3(\text{H}_2\text{O})_3]_n \cdot n\text{H}_2\text{O}$ (dipic = pyridine-2,6-dicarboxylate and $x = 0, 0.1, 0.3, 0.5, 0.7, 0.9$ and 1) were obtained from the reaction mixture 80 mL of water, 6.4 mmol (169.6 mg) of H_2dipic and 1.44 mmol (484.6 mg) of Nd_2O_3 and 0.16 mmol (56.3 mg) of Eu_2O_3 for **(1)**, 1.12 mmol (376.9 mg) of Nd_2O_3 and 0.48 mmol (168.9 mg) of Eu_2O_3 for **(2)**, 0.8 mmol (269.2 mg) of Nd_2O_3 and 0.8 mmol (281.5 mg) of Eu_2O_3 for **(3)**, 0.48 mmol (161.5 mg) of Nd_2O_3 and 1.12 mmol (394.1 mg) of Eu_2O_3 for **(4)**, 0.16 mmol (53.8 mg) of Nd_2O_3 and 1.44 mmol (506.7 mg) of Eu_2O_3 for **(5)**, 1.6 mmol (563.0 mg) of Eu_2O_3 for **(6)**, and 1.6 mmol (538.4 mg) of Nd_2O_3 for **(7)**, in a Teflon[®] reactor and heated at 180 °C for 72 h and then cooled at room temperature. The solid products were washed with water and acetone and dried in a desiccator under reduced pressure.

$[(\text{Nd}_{0.9}\text{Eu}_{0.1})_2(\text{dipic})_3(\text{H}_2\text{O})_3]_n \cdot n\text{H}_2\text{O}$ **(1)**. Yield: 95.5 %. Elemental analysis (%) Calc. for $\text{C}_{21}\text{H}_{16}\text{N}_3\text{O}_{15.5}\text{Nd}_{1.8}\text{Eu}_{0.2}$ (848.3): C, 29.7; H, 0.83; N, 5.0;. Found: C, 28.4; H, 2.0; N, 4.5.

$[(\text{Nd}_{0.7}\text{Eu}_{0.3})_2(\text{dipic})_3(\text{H}_2\text{O})_3]_n \cdot n\text{H}_2\text{O}$ **(2)**. Yield: 92.8 %. Elemental analysis (%) Calc. for $\text{C}_{21}\text{H}_{16}\text{N}_3\text{O}_{15.5}\text{Nd}_{1.4}\text{Eu}_{0.6}$ (851.6): C, 29.6; H, 0.82; N, 4.9;. Found: C, 28.7; H, 1.8; N, 4.5.

$[(\text{Nd}_{0.5}\text{Eu}_{0.5})_2(\text{dipic})_3(\text{H}_2\text{O})_3]_n \cdot n\text{H}_2\text{O}$ **(3)**. Yield: 89.7 %. Elemental analysis (%) Calc. for $\text{C}_{21}\text{H}_{16}\text{N}_3\text{O}_{15.5}\text{NdEu}$ (854.5): C, 29.5; H, 0.82; N, 4.9;. Found: C, 29.0; H, 1.8; N, 4.7.

$[(\text{Nd}_{0.3}\text{Eu}_{0.7})_2(\text{dipic})_3(\text{H}_2\text{O})_3]_n \cdot n\text{H}_2\text{O}$ **(4)**. Yield: 90.7 %. Elemental analysis (%) Calc. for $\text{C}_{21}\text{H}_{16}\text{N}_3\text{O}_{15.5}\text{Nd}_{0.6}\text{Eu}_{1.4}$ (857.6): C, 29.4; H, 0.82; N, 4.9;. Found: C, 28.5; H, 2.0; N, 4.7.

$[(\text{Nd}_{0.1}\text{Eu}_{0.9})_2(\text{dipic})_3(\text{H}_2\text{O})_3]_n \cdot n\text{H}_2\text{O}$ **(5)**. Yield: 81.7 %. Elemental analysis (%) Calc. for $\text{C}_{21}\text{H}_{16}\text{N}_3\text{O}_{15.5}\text{Nd}_{1.8}\text{Eu}_{0.2}$ (860.7): C, 29.3; H, 0.81; N, 4.9;. Found: C, 28.0; H, 2.0; N, 4.5.

$[\text{Eu}_2(\text{dipic})_3(\text{H}_2\text{O})_3]_n \cdot n\text{H}_2\text{O}$ **(6)**. Yield: 98.1 %. Elemental analysis

(%) Calc. for $\text{C}_{21}\text{H}_{16}\text{N}_3\text{O}_{15.5}\text{Eu}_2$ (862.2): C, 29.2; H, 0.81; N, 4.9. Found: C, 31.8; H, 2.3; N, 4.9. $[\text{Nd}_2(\text{dipic})_3(\text{H}_2\text{O})_3]_n \cdot n\text{H}_2\text{O}$ **(7)**. Yield: 98.3 %. Elemental analysis (%) Calc. for $\text{C}_{21}\text{H}_{16}\text{N}_3\text{O}_{15.5}\text{Nd}_2$ (846.85): C, 29.8; H, 0.83; N, 5.0;. Found: C, 32.2; H, 2.5; N, 5.0.

Experimental methods

General instrumentation. Elemental analysis was performed using a Leco Analyser, model CHN 628 and the elemental composition of Nd and Eu were determined in an energy dispersive X-ray spectrometer, model EDX-720. Infrared spectra were recorded with a Shimadzu Spectrum FTIR spectrophotometer, model IR Prestige-21, in the range of 400-4000 cm^{-1} and resolution of 4 cm^{-1} , using the conventional KBr technique. The porosity characteristics of **(1)**–**(7)** compounds were determined by N_2 adsorption–desorption experiments performed at 77 K on NOVA 1200 analyzer. The specific surface area (S_{BET}) was determined from the linear part of the Brunauer-Emmett-Teller (BET) equation.³⁹ Pore size distribution was estimated from the adsorption branch of the isotherm by the Barrett-Joyner-Halenda (BJH) method.⁴⁰ Diffraction data were collected on a Bruker CCD SMART APEX II single crystal diffractometer with Mo $\text{K}\alpha$ radiation (0.71073 Å) at 296K. The data were processed with SAINT and were corrected for absorption using SADABS.⁴¹ The structures were solved by direct methods using SHELXS-97 and subsequent Fourier-difference map analyses yielded the positions of the non-hydrogen atoms. The refinement was performed using SHELXL-97.⁴² X-ray powder diffraction analyses were performed at room temperature, using a Bruker D8 Advanced with Da Vinci design and equipped with a LynxEye Linear Position Sensitive Detector and a Copper (Cu) sealed tube ($\lambda\alpha_1 = 1.5404$ Å, $\lambda\alpha_2 = 1.5444$ Å, $I\alpha_2/I\alpha_1 = 0.5$). Intensity data were collected in step scanning mode, ranging from 5 to 50° (2 θ), with a step size of 0.01°, Soller slit with 2.5° of divergence, 0.5° scattering slit and 0.6 mm receiving slit. The photoluminescence spectra and lifetime measurements were collected using a spectrofluorimeter FLUOROLOG 3 ISA/Jobin-Yvon equipped by double excitation: 450 W Xe arc lamp and a xenon flash arc lamp. The lifetimes were obtained by fitting of integrated photo-luminescence decay curves with a multiexponential function where I_0 is the intensity at $t = 0.01$ ms, A_i is amplitude and τ_i is the lifetime.

$$I(t) = I_0 + \sum_{i=1}^n A_i \exp(-t/\tau_i) \quad (1)$$

The measurements at 10K was performed using a Janis cryostat CCS 400 with Lake Shore 335 temperature controller coupled to the spectrofluorimeter for data acquisition.

Results and Discussion

The single-crystal X-ray diffraction investigation has been performed for **(6)** and **(7)** compounds. These compounds are isostructural to those previously reported by Brouca-Cabarrecq *et al.*⁴³, showing 3D structure and crystallize in the

monoclinic space group $P2_1/c$ (Table S1, ESI). Each asymmetric unit of $[(Nd_{1-x}Eu_x)_2(dipc)_3(H_2O)_3]_n \cdot nH_2O$ ($x = 0, 0.1, 0.3, 0.5, 0.7, 0.9$ and 1) materials comprises two crystallographically independent lanthanide atoms Ln(1) and Ln(2), three crystallographic independent dipc ligands and three coordinated water molecules (Figure S1†). The Ln(1) atom is coordinated by six oxygen and two nitrogen atoms from dipc ligand and another oxygen atom from one coordinated water molecule, resulting in polyhedral Ln(1)O₇N₂ (Figure 1(a)). Ln(2) is bonded to five oxygen and one nitrogen atoms from dipc ligand and two other oxygen atoms from two coordinated water molecules, resulting in polyhedral Ln(2)O₇N (Figure 1(b)). In addition, these coordinated polyhedrons may be described as monocapped square antiprism distorted to ideal symmetry C_{4v} and dodecahedron distorted to ideal symmetry D_{2d} , respectively to the Ln(1) and Ln(2) atoms. The O–Ln–O bond range from $64.02(11)$ – $154.31(10)^\circ$. The Ln–O bond lengths vary from $2.333(3)$ to $2.558(3)$ Å, and the Ln–N distance are in the range of $2.565(4)$ – $2.619(3)$ Å. The crystallographically independent Ln³⁺ ions are interconnected by carboxylate groups of the dipc ligand, which adopts four distinct coordination modes: monodentate, chelating, bimonodentate and $\mu_{1,1}$ -oxo-bridge (see Fig. S1†). This results in a 3D framework, in which present columns linked to each other by intermediate of a carboxylate group (see Fig. S2†) and one-dimensional channels running along the c axis (figure 1(c)). Confirmation of the crystal phase and purity of all compounds synthesized was determined by CHN, FTIR, TGA and X-ray powder diffraction analysis (see support information).

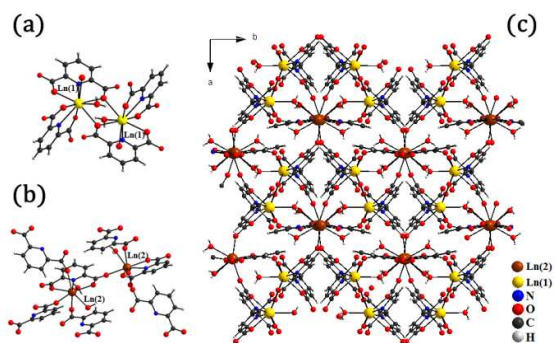


Figure 1: Coordination environment of (a) Ln(1) and (b) Ln(2), and (c) view crystalline structure along the c axis of the extended structure.

The isotherms of N₂ adsorption-desorption at 77K for (1)–(6) compounds and the surface areas, pore volume and pore size data are shown in Figure S3† and Table S2†, respectively (see supporting information). The isotherm format is the type of solid porosity, therefore the coordination polymers have type III isotherm. This isotherm occurs in a few solid porous or macroporous adsorption corresponding to multiple superimposed layers, since the amount adsorbed tends to infinity when P/P_0 tends to 1. In this isotherm type, the isothermal interaction of adsorbate-adsorbent is low, ie the adsorbate molecules (N₂) have greater interaction with each other than with the coordination polymers.⁴⁴ Analyzing the

surface area values, volume and pore size is observed that the materials are classified as microporous, that according to the classification of the IUPAC, have pore diameters less than 20 Å.⁴⁵

The photoluminescent properties of the (6) compound, in solid state and at 10K are presented in Figure 2. The excitation spectrum (solid-black line of Figure 2) was acquired while monitoring the $^5D_0 \rightarrow ^7F_2$ transition of the Eu³⁺ ion at 615 nm. This spectrum shows one broadband between 270 and 350 nm, centred at 303 nm. We can assign this band to electronic transitions $\pi \rightarrow \pi^*$ from aromatic rings of the dipc ligands, according to previous reports.^{46, 47} The thin bands observed between 350 and 600 nm range arise from the intraconfigurational 4f-4f transitions of the Eu³⁺ ions. This spectral profile, with the intensity of bands assigned to dipc ligands is small relative to the intensity of $f-f$ transitions of Eu³⁺ ions and the absence of luminescence assigned to ligands, suggesting that the ion sensitization process through of ligand is effective however less efficient than direct excitation to ion. The emission spectrum (solid-red line of Figure 2) displays typical narrow bands characteristic to the Eu³⁺ ions due to intraconfigurational $^5D_0 \rightarrow ^7F_J$ ($J = 0, 1, 2, 3$ and 4) transitions. The $^5D_0 \rightarrow ^7F_2$ transition (at 615 nm), namely hypersensitive, present five deconvoluted peaks (see Figure S4†) and was primarily responsible for reddish colour of the photoluminescence (56% of the integrated spectrum). The presence of one symmetrical band associated to the $^5D_0 \rightarrow ^7F_0$ transition (578 nm) and full width at half maximum (FWHM) of 48 cm^{-1} , indicates the existence of only one emitting species responsible for this emission band.⁴⁸ According to the selection rules, its presence in the emission spectra may be attributed to the J-mixing of 7F_0 with 7F_2 , and 7F_4 and 7F_6 states.⁴⁸⁻⁵⁰ The $^5D_0 \rightarrow ^7F_0$ transition is observed for the Eu³⁺ ion in systems with coordination environment with local symmetry of type C_s , C_1 , C_n or C_{nv} or distortions of other symmetry in direction to these groups.⁵¹ The data of crystallography show two distinct coordination environment with symmetry C_{4v} for Eu(1) and D_{2d} for Eu(2). The emission spectrum from individual sites cannot be recorded independently from each other even at time resolved measurement and selective excitation even at time resolved measurement (see Figures S13†, S14†, S15† and S16†). Nevertheless, the main responsible for emission characteristics of this material, according to the split profile presented by emission spectrum, is due to Eu(1) with site symmetry C_{4v} (see Figure S4†).^{52, 53} The monoexponential profile presented for lifetime of excited state for the (6) compound (see Fig. S5†), corroborate with this hypothesis.

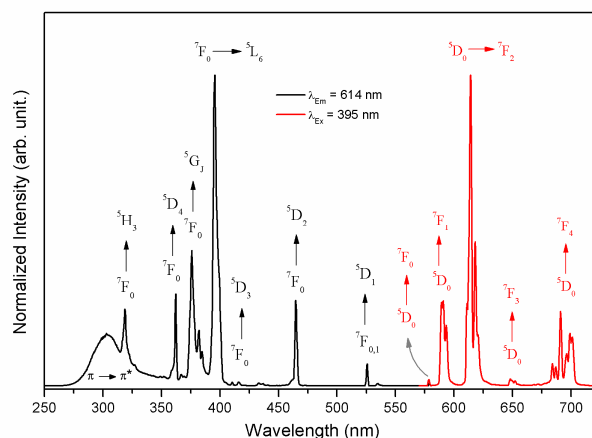


Figure 2: Excitation (solid black line) and emission (solid red line) spectra, at 10K, of (6) compound. Excitation spectrum, was acquired by monitoring ${}^5D_0 \rightarrow {}^7F_2$ transition (615 nm) and emission spectra, were performed upon excitation at 395 nm (${}^7F_0 \rightarrow {}^5L_6$).

The possibility of distortions from symmetry of Eu(2) was considered, but we did not find symmetry correlated to reproduce the split profile of experimental emission spectrum (see Figure S4[†]).⁵³ Thus, we can assign absence of luminescence from Eu(2) ion to symmetry of coordination environment, quenching effect due oscillators O-H of two water molecule directly bonded to Eu(2) ion, energy migration between excited states of Eu(1) and their neighbourhood Eu(2), and concentration quenching of europium ions.^{54, 55}

The emission quantum efficiency (η) of the 5D_0 emitting level from Eu^{3+} ion, is given by equation:^{56, 57}

$$\eta = \frac{A_{\text{rad}}}{A_{\text{total}}} \quad (2)$$

The total decay rate of spontaneous emission is $A_{\text{total}} = (1/\tau) = A_{\text{rad}} + A_{\text{nrad}}$, where $A_{\text{rad}} (= \sum_j A_{0 \rightarrow j})$ and A_{nrad} are the radiative and non-radiative rates, respectively. The coefficients $A_{0 \rightarrow j}$ are determined by taking the magnetic dipole ${}^5D_0 \rightarrow {}^7F_1$ transition as an internal standard since $A_{0 \rightarrow 1}$ rate is almost insensitive to changes in the chemical environment around the europium ion. The spontaneous emission A_{01} is given from emission spectra and can be estimated according to the equations (3), where σ_j is the respective barycenter energy and n is the refraction index.^{57, 58}

$$A_{01} = 0.31 \cdot 10^{-11} \cdot n \cdot (\sigma_j)^3 \quad (3)$$

It was assumed that the n would be equal to 1.5. Others spontaneous emission coefficients A_{0j} ($J = 0, 2, 3$ and 4) were obtained by:⁵⁶⁻⁵⁸

$$A_{0 \rightarrow j} = A_{0 \rightarrow 1} \frac{S_{01} \sigma_{0 \rightarrow j}}{S_{0j} \sigma_{0 \rightarrow 1}} \quad (4)$$

where S_{01} and S_{0j} are the integrated intensities of the ${}^5D_0 \rightarrow {}^7F_1$ and ${}^5D_0 \rightarrow {}^7F_j$ ($J = 0, 2, 3$ and 4) transitions, and σ_{01} and σ_{0j} are their barycentre energies, respectively.

The experimental values of radiative and non-radiative rates of the spontaneous emission (A_{rad} and A_{nrad} , respectively) and quantum efficiency (η) for (6) are summarized in Table 1. The high value for experimental non-radiative rate ($A_{\text{nrad}} = 1811.5 \text{ s}^{-1}$), relative to radiative rate ($A_{\text{rad}} = 316.2 \text{ s}^{-1}$), the low quantum efficiency ($\eta = 15 \%$) and the short lifetime τ (0.47 ms) can be associated to the non-radiative decay channels controlling the relaxation process from the vibronic coupling and O–H oscillators from the water molecules coordinated to the Eu^{3+} ions.⁵⁵

Table 1: Radiative (A_{rad}) and non-radiative (A_{nrad}) decay rates and quantum efficiency (η) for (6) compound.

$A_{\text{rad}} (\text{s}^{-1})$	$A_{\text{nrad}} (\text{s}^{-1})$	τ (ms)	η (%)
316.2	1811.5	0.47	15

The photoluminescence behaviour, in solid state and at room temperature of the (7) compound, was performed by monitoring emission in the near-infrared (NIR) and visible (VIS) spectral range. Excitation spectrum in the VIS range was acquired by monitoring emission at 440 nm (see Figure S6[†]). This spectrum shows three broad bands with maximums at 320, 343 and 370 nm. These bands are assigned to $\pi \rightarrow \pi^*$ transitions from aromatic ring of the dmpc ligands.

Monitoring emission in the NIR range (1060 nm), the excitation spectrum present the band assigned to $\pi \rightarrow \pi^*$ transition of dmpc ligand between 250 and 320 nm (see Figures S7, ESI). The bands between 320 and 800 nm were assigned to ${}^4I_{11/2} \rightarrow {}^2I_{13/2}$ (326 nm), ${}^4D_{5/2, 3/2, 1/2}$ (350 nm), ${}^2P_{3/2}$ (378 nm), ${}^2P_{1/2}$ (424 nm), ${}^2K_{15/2}$ and ${}^4G_{11/2}$ (463 nm), ${}^2K_{13/2}$ and ${}^4G_{9/2}$ (507 nm), ${}^4G_{7/2, 5/2}$ (519 nm), ${}^2G_{7/2, 5/2}$ (576 nm), ${}^2H_{11/2}$ (621 nm), ${}^4F_{9/2}$ (674 nm), ${}^4F_{7/2}$ and ${}^4S_{3/2}$ (731 nm), and ${}^4F_{5/2}$ and ${}^2H_{9/2}$ (nm) (793 nm) transitions of Nd^{3+} ions (see Figure S7[†]).⁵⁹

The emission spectra in the NIR and VIS range were performed upon excitation at 350 and 370 nm, respectively, and are depicted in Figure 3. The NIR emission spectra (solid-black line of Figure 3), display two characteristic emission bands centred at 1060 and 1345 nm, which correspond to ${}^4F_{3/2} \rightarrow {}^4I_{11/2}$ and ${}^4F_{3/2} \rightarrow {}^4I_{13/2}$ electronic transitions of Nd^{3+} ions, respectively. In the visible range, the emission spectra present verified hump bands from 400 to 600 nm and are assigned to $\pi^* \rightarrow \pi$ transitions from dmpc ligand. This interference is attributed to self-absorption of emission by Nd^{3+} ions, from ground state ${}^4I_{11/2}$ to excited states ${}^2D_{5/2}$, ${}^2P_{1/2}$, ${}^4G_{11/2}$, ${}^3K_{13/2}$, ${}^4G_{9/2, 7/2, 5/2}$, ${}^4G_{7/2, 5/2}$ and ${}^2H_{11/2}$ as depicted in Figure 4. Similar behaviour has been reported by Silva and co-workers, at low temperature, in the poly(styrene sulfonate) (PSS) films doped with Nd^{3+} ions.⁶⁰ In addition, this data shows the possible energy transference from dmpc ligand by other mechanisms.

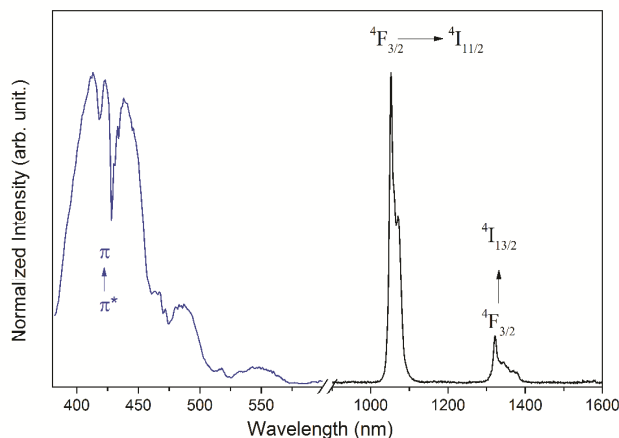


Figure 3: Emission spectra of (7) compound, at room temperature, upon excitation at 370 nm.

The radiative lifetime of excited state was obtained upon excitation at 370 nm and 350 nm, by monitoring emission at 440 and 1060 nm, respectively. Decay curves of this coordination polymer could be fitted mono-exponentially (See Figures S8† and S9†). This short lifetime for emission in 1060 nm corresponds high incidence to non-radiative deactivation processes (quenching effects) most probably to O-H, C-H oscillators, vibronic mechanisms and cross-relaxation on intermediate levels (${}^4F_{3/2} \rightarrow {}^4I_{15/2}$)-(${}^4I_{9/2} \rightarrow {}^4I_{15/2}$).^{21, 55, 61-63}

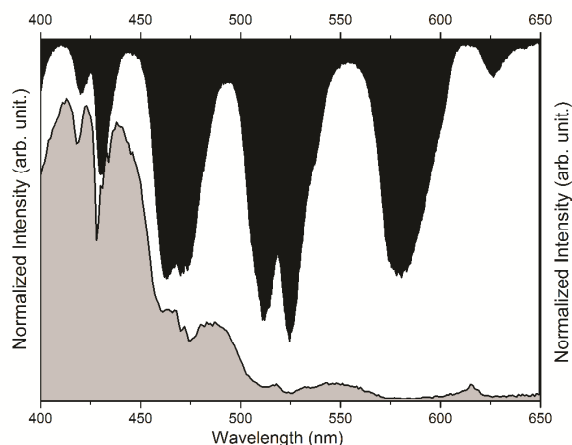


Figure 4: Excitation and emission spectra of (7) compound shows interference effect caused by absorption of Nd^{3+} ion. The emission spectrum (light gray area) was acquired upon excitation in 370 nm. The excitation spectrum (dark gray area), was performed by monitoring emission at 1060 nm (${}^4I_{11/2} \rightarrow {}^4F_{3/2}$) and intensity data multiplied for (λ^{-1}) .

The NIR and VIS photoluminescence in solid state of (1)-(5) materials, are performed at room temperature. The excitation spectra of these compounds, monitoring emission at 440 ($\pi^* \rightarrow \pi$), 615 (${}^5D_0 \rightarrow {}^7F_2$) and 1060 nm (${}^4F_{3/2} \rightarrow {}^4I_{11/2}$), corresponding to emission of dipic ligand, Eu^{3+} and Nd^{3+} ions, respectively, were performed and depicted in Figures S10† and S11† (see support information) and in Figure 5. In Figure S11†, we observed that increasing concentration of Eu^{3+} ion, relative to concentration of Nd^{3+} ion, was verified the pronounced increasing of the interference effect caused by Nd^{3+} ion in the

emission profile due to self-absorption from emission of the dipic ligand, as discussed above for the (7) compound. Regarding excitation spectra when monitoring emission at 615 nm (${}^5D_0 \rightarrow {}^7F_2$ of Eu^{3+} ions) (Figure S11†), we found that with increased concentration of Eu^{3+} ions, relative to Nd^{3+} ion, the intensity of bands due $f-f$ and $\pi \rightarrow \pi^*$ transitions of Eu^{3+} ion dipic ligand, respectively, are increasing. This behaviour revealing the existence of crystallographic doming containing distinct population of only Eu^{3+} ion, and which first band observed at 320 nm from excitation spectra of (7) compound is due to absorption of the ligands coordinated to Ln(1) atom, with symmetry C_{4v} and responsible for red emission to (6) compound.

Figure 5 shows excitation spectra of (1)-(5) materials by monitoring emission at 1060 nm (${}^4F_{3/2} \rightarrow {}^4I_{11/2}$). Characteristic absorption bands of Nd^{3+} ion due to transitions from ground-state ${}^4I_{11/2}$ to excited states were assigned. In addition, others bands were marked with asterisks symbol.

The relative intensity of these bands marked with asterisk symbol increases progressively, in detriment to $f-f$ transitions of Nd^{3+} ions, with increase to proportion of Eu^{3+} ion. We can assign these bands to transitions ${}^7F_0 \rightarrow {}^5G_1$ (380 nm), 5L_6 (394 nm), 5D_2 (464 nm) and 5D_1 (534 nm) of Eu^{3+} ion and reveal the energy transfer channels from Eu^{3+} to Nd^{3+} ions.

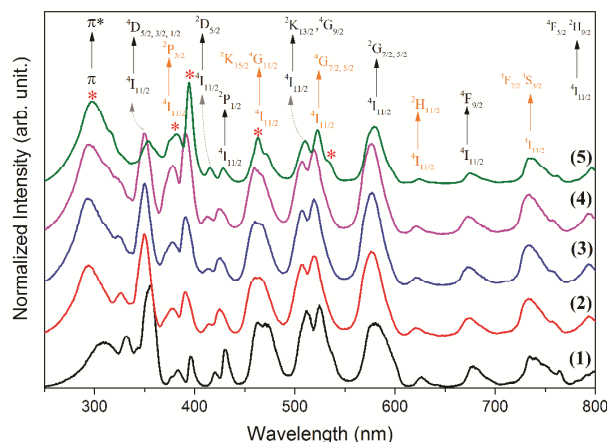


Figure 5: Excitation spectra of (1)-(5) compound, acquired by monitoring emission at 1060 nm (${}^4F_{3/2} \rightarrow {}^4I_{11/2}$ transition).

Figure 6 presents the emission spectra, at room temperature, of (1)-(5) compounds in the NIR and VIS range, upon excitation at 300 and 350 nm. The emission spectra of these materials upon excitation at 350 nm are depicted by the blue and black lines. In the VIS range, these emission spectra shows the maintenance from the profile of emission bands to dipic ligand previously presented for (7) compound. The absence of emission bands from Eu^{3+} ions is due to complete quenching caused by energy transfer (ET) among the donor centre Eu^{3+} ion and acceptor centre Nd^{3+} ion, as reported in the literature for several materials.^{64, 65} However, in the (4) and (5) compounds we observe small bands between 570 and 715 nm

assigned to ${}^5D_0 \rightarrow {}^7F_J$ ($J = 0, 1, 2, 3$ and 4) transitions of Eu^{3+} ion. This behaviour results from the randomized distribution and formation of distinct populations to Ln^{3+} ions in these materials, as discussed above. In the NIR range, the emission spectra are similar to those presented by the (7) compound when it is excited at 370 nm (see figure S12[†]).

The excitation at 300 nm corresponds to sensitization of Eu^{3+} and Nd^{3+} ions by dpcp ligand, resulting a verify change in the emission spectra profile (solid red line of Figure 6) in the visible spectral range, relative to excitation at 350 nm, of the (1)-(5) materials. For the (1) and (5) compounds, practically don't verify emission to $\pi^* \rightarrow \pi$ transition of dpcp ligand. The emission of ligand is verified for (2), (3) and (4) compounds, together with $f-f$ transitions of Eu^{3+} ions well defined. These behaviours corroborate the hypothesis to existence of distinct populations of Ln^{3+} , due to randomized distribution from Nd^{3+} and Eu^{3+} ions. In addition, we verified the appearance of emissions from excited state 5D_1 to ground states 7F_J ($J = 0, 1$ and 2). This behaviour is attributed to concentration effect, since the strong interaction between ions and a cross-relaxation process can explain the quenching effect due to fast decay from 5D_1 (19085 cm^{-1}) state to 5D_0 (17182 cm^{-1}) state in (6) materials most probably by $({}^5D_1, {}^7F_0) \rightarrow ({}^5D_0, {}^7F_3)$ although phonon assisted $({}^5D_1, {}^7F_0) \rightarrow ({}^5D_0, {}^7F_4)$ and $({}^5D_1, {}^7F_1) \rightarrow ({}^5D_0, {}^7F_4)$ is possible at room temperature.⁵⁴

The emission spectra of (1)-(5) materials, have demonstrated dependence of the excitation wavelength, mainly to visible spectral range, since the relative amplitude of the emission transitions have shown substantial alterations upon distinct excitation. These results indicate that these materials are promising applications in photonic devices, with emission in distinct spectral regions as a function of excitation wavelength.

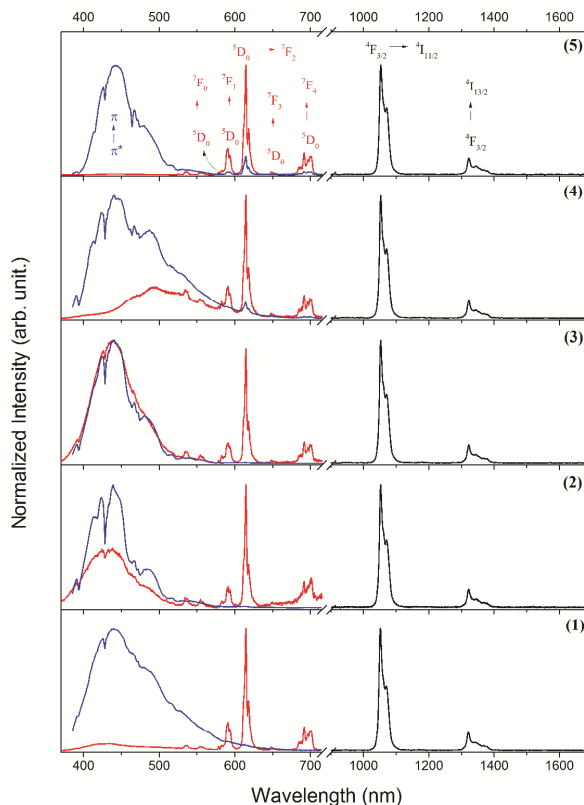


Figure 6: Emission spectra of (1)-(5) compounds in the VIS-NIR spectral range, upon excitation at 300nm (solid red line) and 350 nm (solid blue and black lines)

According to the above experimental results, the schematic energy level diagram and possible process to energy transfer and emission for (1)-(5) compounds are shown in Figure 7. According to literature data, the excited states of the dpcp ligand (π^*) are higher than the ${}^4F_{3/2}$ and 5D_0 emissive levels of Nd^{3+} and Eu^{3+} ions, respectively.^{46, 66} Although the first triplet excited level of the dpcp ligand presents energy too high relative to the emitting levels of these ions for allowing an effective back energy transfer, losses take place during the energy transfer from others upper excited states to emitting levels due to other processes such as vibronic mechanism, O-H and C-H oscillators and cross-relaxation. The process to the deactivation of excited states of these mix-lanthanide-organic systems by the sensitization of dpcp ligand, operate by cascade of energy transfer. In the first step, the initially populated states (π^*) of the dpcp ligand may decay by two processes: i) radiative decay for ground state (π) (blue spectral range) or ii) energy transfer to excited states of the Eu^{3+} or Nd^{3+} ions (antenna effect). In the second step, the deactivation of excited states of Eu^{3+} ion may occur by radiative decay with emission in red spectral range or non-radiative decay by energy transfer for the excited states of the Nd^{3+} ion. In turn, the excited state (${}^4F_{3/2}$) of Nd^{3+} ion decay for ground state 4I_J , occurs with emission in the NIR range. After the second process of the first step, the metastable ${}^4F_{3/2}$ level of Nd^{3+} ion decay for ground state 4I_J ($J = 11/2$ and $13/2$) with emission in

the NIR range. In addition, we verified to absorption of emission to dipc ligand (blue range) and Eu^{3+} ion (red range) by the Nd^{3+} ions. Summarizing, verify that excitation of the ligand-centred, $\pi \rightarrow \pi^*$ transitions, in (1)–(5) coordination polymers gives a luminescence with three components, including the residual ligand-centered $\pi^* \rightarrow \pi$ in the blue range, and emissions in the red and NIR range by Eu^{3+} and Nd^{3+} ions, respectively.

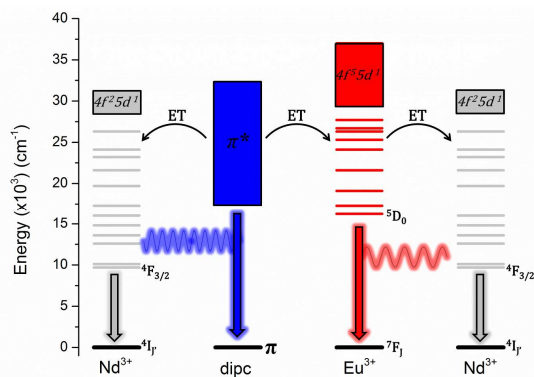


Figure 7. Schematic energy level diagram and energy transfer process for (1)–(5) compounds. $^4I_9/2$ and $^4F_{3/2}$ are ground and first excited states of Nd^{3+} ion; π and π^* are ground and excited states of dipc ligand, respectively; 7F_1 and 5D_0 are ground and first excited states of Eu^{3+} ; arrows, represents emission of light; dotted arrows, represent non-radiative transfer energy between excited states of Nd^{3+} , Eu^{3+} and dipc ligand; wavy blue line, represents absorption of emission from ligand by Nd^{3+} ion; wavy red line represents absorption of emission from ligand by Eu^{3+} ion.

Conclusions

In the present study, the five new heteronuclear and other two homonuclear coordination polymers were obtained for hydrothermal routing. Compound (6) displays emission primarily of the $\text{Eu}(1)$ centre with C_{4v} symmetry. The absent of emission to $\text{Eu}(2)$ is due to its symmetry and non-radiative deactivation process. Compound (7), show emission in the blue and NIR spectral range. The heteronuclear (1)–(5) materials display emission in the VIS and NIR range, and present dependencies of the excitation wavelength, mainly to visible spectral range, with substantial alterations upon distinct excitation. Thus, the compounds (1)–(5) present double emission (VIS and NIR range) tunable in the VIS (blue or red) spectral range. The tuning of emission on the red or blue range may be performed by stoichiometric ratio control between the lanthanide ions and by excitation wavelength. This dependence with excitation wavelength confers to these materials promising applications in photonic devices. The Eu^{3+} ions acting as efficient sensitizer to Nd^{3+} ions becomes the main sensitization channel to the Nd^{3+} ions, in the (5) compound. Nd^{3+} ions present self-absorption of emission to dipc ligand in (1)–(5) and (7) coordination polymers.

Acknowledgements

The authors gratefully acknowledge CNPq (INCT/INAMI and RH-INCT/INAMI, FACEPE and CAPES for its financial support.

References

- D. Ma, B. Li, X. Zhou, Q. Zhou, K. Liu, G. Zeng, G. Li, Z. Shi and S. Feng, *Chem. Commun.*, 2013, **49**, 8964–8966.
- Z. Hu, B. J. Deibert and J. Li, *Chem. Soc. Rev.*, 2014, **43**, 5815–5840.
- W. Xie, S.-R. Zhang, D.-Y. Du, J.-S. Qin, S.-J. Bao, J. Li, Z.-M. Su, W.-W. He, Q. Fu and Y.-Q. Lan, *Inorg. Chem.*, 2015.
- Y. Zheng, S.-H. Wang, S.-F. Wu, F.-K. Zheng and A. Q. Wu, *Inorg. Chem. Commun.*, 2015, **53**, 20–22.
- K.-Y. A. Lin and H.-A. Chang, *Journal of the Taiwan Institute of Chemical Engineers*.
- M. C. So, G. P. Wiederrecht, J. E. Mondloch, J. T. Hupp and O. K. Farha, *Chem. Commun.*, 2015, **51**, 3501–3510.
- Y. Li, S. Zhang and D. Song, *Angew. Chem. Int. Ed.*, 2013, **52**, 710–713.
- C. Feng, J.-W. Sun, P.-F. Yan, Y.-X. Li, T.-Q. Liu, Q.-Y. Sun and G.-M. Li, *Dalton Transactions*, 2015, **44**, 4640–4647.
- X.-N. Zhang, L. Liu, Z.-B. Han, M.-L. Gao and D.-Q. Yuan, *RSC Advances*, 2015, **5**, 10119–10124.
- Y. Cui, B. Chen and G. Qian, *Coord. Chem. Rev.*, 2014, **273–274**, 76–86.
- E. van der Kolk, P. Dorenbos, K. Krämer, D. Biner and H. U. Güdel, *Physical Review B*, 2008, **77**, 125110.
- A. D'Aléo, F. Pointillart, L. Ouahab, C. Andraud and O. Maury, *Coord. Chem. Rev.*, 2012, **256**, 1604–1620.
- S. V. Eliseeva and J.-C. G. Bunzli, *Chem. Soc. Rev.*, 2010, **39**, 189–227.
- J.-C. G. Bunzli and S. V. Eliseeva, *Journal of Rare Earths*, 2010, **28**, 824–842.
- E. Deiters, B. Song, A.-S. Chauvin, C. D. B. Vandevyver and J.-C. G. Bunzli, *New J. Chem.*, 2008, **32**, 1140–1152.
- J.-C. G. Bunzli and C. Piguet, *Chem. Soc. Rev.*, 2005, **34**, 1048–1077.
- S. V. Eliseeva and J.-C. G. Bunzli, *New J. Chem.*, 2011, **35**, 1165–1176.
- M. Venkateswarlu, S. Mahamuda, K. Swapna, M. V. V. K. S. Prasad, A. Srinivasa Rao, A. Mohan Babu, S. Shakya and G. Vijaya Prakash, *Opt. Mater.*, 2015, **39**, 8–15.
- D. Avram, C. Gheorghie, C. Rotaru, B. Cojocar, M. Florea, V. Parvulescu and C. Tiseanu, *J. Alloys Compd.*, 2014, **616**, 535–541.
- Y. Cui, Y. Yue, G. Qian and B. Chen, *Chem. Rev.*, 2012, **112**, 1126–1162.
- K. Shinozaki, T. Honma and T. Komatsu, *Opt. Mater.*, 2014, **36**, 1384–1389.
- Li, Y. A.; Ren, S. K.; Liu, Q. K.; Ma, J. P.; Chen, X.; Zhu, H.; Dong, Y. B. *Inorg. Chem.* **2012**, **51**, 9629.
- Jiang, Y. Y.; Ren, S. K.; Ma, J. P.; Liu, Q. K.; Dong, Y. B. *Chemistry* **2009**, **15**, 10742.
- Wang, P.; Ma, J. P.; Dong, Y. B. *Chemistry* **2009**, **15**, 10432.
- S.-N. Zhao, L.-J. Li, X.-Z. Song, M. Zhu, Z.-M. Hao, X. Meng, L.-L. Wu, J. Feng, S.-Y. Song, C. Wang and H.-J. Zhang, *Adv. Funct. Mater.*, 2015, **25**, 1463–1469.
- D. K. Singha, P. Majee, S. K. Mondal and P. Mahata, *Eur. J. Inorg. Chem.*, 2015, **2015**, 1390–1397.
- Y. Wei, R. Sa, Q. Li and K. Wu, *Dalton Transactions*, 2015, **44**, 3067–3074.

28. C. Zhan, S. Ou, C. Zou, M. Zhao and C.-D. Wu, *Anal. Chem.*, 2014, **86**, 6648-6653.
29. X. Rao, T. Song, J. Gao, Y. Cui, Y. Yang, C. Wu, B. Chen and G. Qian, *J. Am. Chem. Soc.*, 2013, **135**, 15559-15564.
30. D. Ananias, F. A. A. Paz, D. S. Yufit, L. D. Carlos and J. Rocha, *J. Am. Chem. Soc.*, 2015, **137**, 3051-3058.
31. J. Rocha, L. D. Carlos, F. A. A. Paz and D. Ananias, *Chem. Soc. Rev.*, 2011, **40**, 926-940.
32. F. F. da Silva, F. L. de Menezes, L. L. da Luz and S. Alves, *New J. Chem.*, 2014, **38**, 893-896.
33. Z. Wang, Y. Yang, Y. Cui, Z. Wang and G. Qian, *J. Alloys Compd.*, 2012, **510**, L5-L8.
34. M. O. Rodrigues, J. D. L. Dutra, L. A. O. Nunes, G. F. de Sá, W. M. de Azevedo, P. Silva, F. A. A. Paz, R. O. Freire and S. A. Júnior, *The Journal of Physical Chemistry C*, 2012, **116**, 19951-19957.
35. P. P. Lima, O. L. Malta and S. Alves Júnior, *Quím. Nova*, 2005, **28**, 805-808.
36. H. A. Azab, A. Duerkop, Z. M. Anwar, B. H. M. Hussein, M. A. Rizk and T. Amin, *Anal. Chim. Acta*, 2013, **759**, 81-91.
37. A. Fernandes, J. Jaud, J. Dexpert-Ghys and C. Brouca-Cabarrecq, *Polyhedron*, 2001, **20**, 2385-2391.
38. A. Mondry and P. Starynowicz, *J. Alloys Compd.*, 1995, **225**, 367-371.
39. S. Brunauer, P. H. Emmett and E. Teller, *J. Am. Chem. Soc.*, 1938, **60**, 309-319.
40. E. P. Barrett, L. G. Joyner and P. P. Halenda, *J. Am. Chem. Soc.*, 1951, **73**, 373-380.
41. G. i. Sheldrick, *University of Göttingen, Germany*, 1997.
42. G. Sheldrick, *Acta Crystallographica Section A*, 2008, **64**, 112-122.
43. C. Brouca-Cabarrecq, A. Fernandes, J. Jaud and J. P. Costes, *Inorg. Chim. Acta*, 2002, **332**, 54-60.
44. Gregg, S. J.; Sing, K. S. W. Adsorption, Surface Area and Porosity. **Academic Press**, p. 41, 1982.
45. J. Rouquerol, D. Avnir, D. H. Everett, C. Fairbridge, M. Haynes, N. Pernicone, J. D. F. Ramsay, K. S. W. Sing and K. K. Unger, in *Stud. Surf. Sci. Catal.*, eds. F. R.-R. K. S. W. S. J. Rouquerol and K. K. Unger, Elsevier, Editon edn., 1994, vol. Volume 87, pp. 1-9.
46. M. Latva, H. Takalo, V.-M. Mukkala, C. Matachescu, J. C. Rodríguez-Ubis and J. Kankare, *J. Lumin.*, 1997, **75**, 149-169.
47. A. L. Ramirez, K. E. Knope, T. T. Kelley, N. E. Greig, J. D. Einkauf and D. T. de Lill, *Inorg. Chim. Acta*, 2012, **392**, 46-51.
48. H. Wen, G. Jia, C.-K. Duan and P. A. Tanner, *PCCP*, 2010, **12**, 9933-9937.
49. O. L. Malta, W. M. Azevedo, E. A. Gouveia and G. F. de Sá, *J. Lumin.*, 1982, **26**, 337-343.
50. M. Tanaka, G. Nishimura and T. Kushida, *Physical Review B*, 1994, **49**, 16917-16925.
51. X. Y. Chen and G. K. Liu, *J. Solid State Chem.*, 2005, **178**, 419-428.
52. G. M. Murray, R. V. Sarrío and J. R. Peterson, *Inorg. Chim. Acta*, 1990, **176**, 233-240.
53. R. Reisfeld, E. Zigansky and M. Gaft, *Mol. Phys.*, 2004, **102**, 1319-1330.
54. F. Pellé, P. Aschehoug, S. Surblé, F. Millange, C. Serre and G. Férey, *J. Solid State Chem.*, 2010, **183**, 795-802.
55. A. Beeby, I. M. Clarkson, R. S. Dickens, S. Faulkner, D. Parker, L. Royle, A. S. de Sousa, J. A. Gareth Williams and M. Woods, *Journal of the Chemical Society, Perkin Transactions 2*, 1999, 493-504.
56. E. R. dos Santos, R. O. Freire, N. B. da Costa, F. A. A. Paz, C. A. de Simone, S. A. Júnior, A. A. S. Araújo, L. A. O. Nunes, M. E. de Mesquita and M. O. Rodrigues, *The Journal of Physical Chemistry A*, 2010, **114**, 7928-7936.
57. D. Wang, C. Zheng, L. Fan, J. Zheng and X. Wei, *Synth. Met.*, 2012, **162**, 2063-2068.
58. E. E. S. Teotonio, G. M. Fett, H. F. Brito, W. M. Faustino, G. F. de Sá, M. C. F. C. Felinto and R. H. A. Santos, *J. Lumin.*, 2008, **128**, 190-198.
59. E. Antic-Fidancev, F. Serpaggi and G. Férey, *J. Alloys Compd.*, 2001, **319**, 140-144.
60. M. C. Silva, A. S. S. de Camargo, L. A. O. Nunes, R. A. Silva and A. Marletta, *J. Non-Cryst. Solids*, 2008, **354**, 5496-5503.
61. W. Miniscalco, *Lightwave Technology, Journal of*, 1991, **9**, 234-250.
62. F. Artizzu, M. L. Mercuri, A. Serpe and P. Deplano, *Coord. Chem. Rev.*, 2011, **255**, 2514-2529.
63. J.-C. G. Bünzli, *Coord. Chem. Rev.*
64. T. G. V. M. Rao, A. Rupesh Kumar, K. Neeraja, N. Veeraiiah and M. Rami Reddy, *J. Alloys Compd.*, 2013, **557**, 209-217.
65. N. G. Boetti, D. Negro, J. Lousteau, F. S. Freyria, B. Bonelli, S. Abrate and D. Milanese, *J. Non-Cryst. Solids*, 2013, **377**, 100-104.
66. N. Arnaud and J. Georges, *Spectrochimica Acta Part A: Molecular and Biomolecular Spectroscopy*, 2003, **59**, 1829-1840.